

Temporal Glare: Real-Time Dynamic Simulation of the Scattering in the Human Eye

T. Ritschel¹ M. Ihrke² J. R. Frisvad³ J. Coppens⁴ K. Myszkowski¹ H.-P. Seidel¹

¹MPI Informatik

³Technical University of Denmark

²Bernstein Center for Computational Neuroscience, Göttingen

⁴Netherlands Institute for Neuroscience / KNAW

Abstract

Glare is a consequence of light scattered within the human eye when looking at bright light sources. This effect can be exploited for tone mapping since adding glare to the depiction of high-dynamic range (HDR) imagery on a low-dynamic range (LDR) medium can dramatically increase perceived contrast. Even though most, if not all, subjects report perceiving glare as a bright pattern that fluctuates in time, up to now it has only been modeled as a static phenomenon. We argue that the temporal properties of glare are a strong means to increase perceived brightness and to produce realistic and attractive renderings of bright light sources. Based on the anatomy of the human eye, we propose a model that enables real-time simulation of dynamic glare on a GPU. This allows an improved depiction of HDR images on LDR media for interactive applications like games, feature films, or even by adding movement to initially static HDR images. By conducting psychophysical studies, we validate that our method improves perceived brightness and that dynamic glare-renderings are often perceived as more attractive depending on the chosen scene.

Categories and Subject Descriptors (according to ACM CCS): COMPUTER GRAPHICS [I.3.7]: Three-Dimensional Graphics and Realism—; COMPUTER GRAPHICS [I.3.3]: Color, Shading, Shadowing and Texture—

1. Introduction

Glare effects are typical in any optical system used for capturing an image with directly visible bright light sources, caustics, or highlights. Glare is common in our everyday observation of the real world because light scatters in the human eye. Effectively, instead of having a crisp projected image of bright objects on the retina, surrounding regions are affected by scattered light. This leads, among other effects, to local contrast reduction (also called the veiling effect or disability glare). While this is often an unwanted effect in photography [RAWV08], we can exploit it for displaying HDR-content on LDR-devices. When a veiling pattern is painted on the image (as a gradient surrounding the light source), the corresponding retinal image is similar to the observation of a real bright object and is thus interpreted by the human brain as brighter [YIMS08]. This effect has been used by artists for centuries to improve apparent dynamic range of their paintings, and it is just as attractive today in a digital imaging context.

A typical glare pattern for a small light source as perceived

by most subjects with normal eyes is depicted in Fig. 1, but the actual appearance of the glare varies with viewing conditions and observers. In general the effects of glare can be divided into *bloom*, a general loss of contrast in the surroundings of the retinal image of the light-source (veil), and *flare* which comprises the *ciliary corona* (the sharp needles) and the *lenticular halo* surrounding the light [SSZG95]. Although it cannot be reproduced in static images on paper, people usually report that the glare pattern fluctuates in a fluid-like motion when observed under real world conditions. Additionally, flickering of the fine needles forming the *ciliary corona* is readily observable and many people perceive a pulsation of the glare intensity. While these effects are striking, glare has previously only been modeled as a static phenomenon. The dynamics we discuss do not occur for cameras but only for eyes. In traditional animation, dynamic glare effects are used for artistic effect.

In this work we investigate temporal aspects of glare appearance and perform simulation of light scattering within the eye based on Fourier optics for high fidelity glare rendering.



Figure 1: Glare effect rendered for a point source using our model. The colorful ring is called the lenticular halo; the fine radiating needles constitute the ciliary corona.

Our goal is not only to render glare realistically with real-time performance, but also to show that by better mimicking the real world experience the image brightness impression and overall perceived quality can be improved. Specific contributions of this work are as follows:

- We develop a model for light scattering in the human eye based on wave-optics. This includes temporal characteristics of major anatomical structures contributing to glare (Section 3).
- We efficiently map this model to current GPU architectures and achieve real time performance (Section 5).
- We perform psychophysical studies to measure the perceived brightness and preference for static and dynamic glare models (Section 6.1).

Following previous work in Section 2, we present our eye model in Section 3, describe its scattering computation in Section 4 and its GPU implementation in 5. We present results in Section 6 before concluding in Section 7.

2. Previous Work

The modeling of glare effects has been used to improve image realism and to convey an impression of high intensity of luminaires in the context of realistic rendering [SSZG95], driving simulation [NKON90], computer games [Kaw05], image post-processing [Rok93], and tone mapping [LRP97, DD00]. A recent perceptual study [YIMS08] demonstrates that the impression of displayed image brightness can be increased by over 20% by convolving high intensity pixels in the

image with relatively simple filters used in glare models [SSZG95, Kaw05]. Precise information about the intensity values of light sources and highlights represented by such pixels is immediately available in 3D image synthesis and HDR photography [RWP05]. For physically based rendering and photometrically calibrated cameras, such pixel intensity can even be properly scaled in cd/m^2 units, which is important for faithful modeling of light scattering in the eye.

The majority of existing approaches to computer-generated glare, while inspired by knowledge about human eye anatomy and physiology, are based on phenomenological results rather than explicit modeling of the underlying physical mechanisms. A common approach is to design convolution filters, which reduce image contrast in the proximity of glare sources up to full image saturation in the glare center. Nakamae et al. [NKON90] derive such a filter to model the light diffraction on the eye pupil and eyelashes for various wavelengths. Spencer et al. [SSZG95] base their filter on the point-spread function (PSF) measured for the optics of the human eye. Glare solutions used in tone mapping [LRP97, DD00] are mostly based on Spencer et al.'s approach. A set of Gaussian filters with different spatial extent, when skillfully applied, may lead to very convincing visual results. This approach is commonly used in computer games [Kaw05] and rendering post-production [RWP05, Section 9.2.5]. Other glare effects such as the ciliary corona and the lenticular halo are often designed off-line, and placed in the location of the brightest pixel for each glare source as a billboard (image sprite) [Rok93, SSZG95]. In the designing of such billboards, seminal ophthalmology references are used such as [Sim53]. The resulting appearance is very realistic for small point-like glare sources. However, using billboards, it is difficult to realistically render glare for glare sources of arbitrary shape and non-negligible spatial extent.

Recently, there have been some successful attempts to model glare based on the principles of wave optics. Kakinoto et al. [KMN*04] propose a practical model to simulate scattering from a single plane rigid aperture. Three diffraction-causing obstacles: the eyelashes, the eyelids, and the pupil edge are placed in this plane. The Fraunhofer diffraction formula is then used to determine the diffraction pattern of the obstacle-plane on the retina. This pattern is stored as a billboard, placed at high-intensity pixels and blended with the rendered image. Similarly, van den Berg et al. [vdBHC05] describe glare as diffraction by particles in the lens. By computing this pattern for multiple wavelengths, they achieve the first physical simulation of the ciliary corona.

To our knowledge, the present work is the first to consider a dynamic eye model that enables us to simulate the temporal fluctuations of glare. Our model is also more complete with respect to existing static models by considering all significant contributions to light scattering in the eye. As an example, we model light scattering on particles in the lens nucleus and vitreous humor as well as the grating-like fiber structure in

the lens cortex (cf. Fig. 2). These greatly contribute to the ciliary corona and the lenticular halo (cf. Fig. 1), but they are ignored by Kakimoto et al.

3. A Dynamic Human Eye Model for Glare

In this section we propose a time-dependent human eye model that is suitable for real-time computation of plausible dynamic glare. We will outline anatomical and physiological characteristics of all parts of the eye that contribute to the light-scattering characteristics of glare. Furthermore, we discuss dynamics shown by these anatomical structures and incorporate their characteristics in our model. Fig. 2 is a schematic diagram of the human eye. From front to back the optically important parts are the cornea, the aqueous humor, the iris and pupil, the lens, the vitreous humor, and the retina. Table 1 summarizes their contribution to scattering, whether they show temporal fluctuations, and whether we include them in our model or not. Multiple scattering is relatively unimportant with respect to glare [vdB95], and, in single scattering, only the light scattered in the forward direction will reach the sensory system. We will therefore only consider forward scattering in the present work. There are large differences between individual eyes and hence in how glare is perceived by different subjects. In this work, we will use data obtained from studies of the normal healthy eye to fit our model.

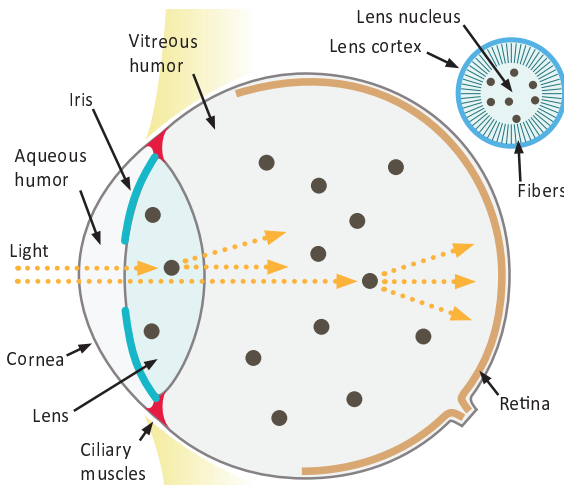


Figure 2: Anatomy of the human eye. The upper-right inset shows the lens structure.

3.1. The Cornea

The main part of the cornea is formed by collagen fibrils which are densely packed, regularly arranged, cylindrically shaped particles [FMF86]. This special arrangement of the fibrils ensures that they are almost transparent [Ben71]. Between the fibrils there is a transparent ground substance, and a few

Eye part	Scatter	Dyn.	Incl.
Eyelashes [KMN*04]	varies	yes	yes
Cornea [VB63, BC64]	25-30%	no	yes
Aqueous humor [WS82]	none	no	no
Lens [YYG*93]	40%	yes	yes
Iris [vdBIdW91]	$\leq 1\%$	yes	no
Pupil [Fry91]	aperture	yes	yes
Vitreous humor [KRFF95]	10%	yes	yes
Retina [VB64]	20%	no	yes

Table 1: An overview of the contribution from each part of the eye to the glare phenomenon and to our model. From left to right, the columns describe: the name of the structure, its scattering (percentages refer to the fraction of the total intraocular scattering); whether it is dynamic or not; and whether it is included in our model or not.

flat cells are interspersed. These flat cells occupy 3–5% of the corneal volume and they have a diameter of $15\mu\text{m}$ [FMF86]. The flat cells contribute to the glare pattern (25–30%, cf. Table 1), but the effect is static. We simulate this by having large, sparsely distributed, static particles in our pupil plane.

3.2. The Iris and Pupil

A very small percentage (1% or less depending on eye color) is scattered through the iris which is tinted due to absorption [vdBIdW91]. We choose to ignore this faint straylight.

The pupil contributes important diffraction to the glare pattern as it is the aperture of our model. The iris muscles have the ability to control the size of the pupil. Exposition to a glare source will typically give rise to the *pupillary hippus*, an involuntary, periodic fluctuation of the pupil size. It is presumably caused by opposing actions of the iris muscles due to the vastly different lighting conditions of glare source and background when attempting to adjust the pupil [MPC02]. Curves describing the pupil diameter as a function of time for different glare source intensities have been measured by Fry [Fry91]. We have found the following expression which mimics these dynamics:

$$h(t, p) = p + \text{noise}\left(\frac{t}{p}\right) \frac{p_{\max}}{p} \sqrt{1 - \frac{p}{p_{\max}}} , \quad (1)$$

where t is time (in seconds), p is the mean pupil diameter (in mm) for a given glare source intensity, p_{\max} is the maximum pupil size (we use $p_{\max} = 9\text{ mm}$), and $\text{noise}(\cdot)$ is a noise function. It remains to map glare source intensity to the mean pupil diameter p . We use the function proposed by Moon and Spencer [MS44]:

$$p = 4.9 - 3 \tanh(0.4(\log L_v + 1)) , \quad (2)$$

where L_v is the field luminance measured in cd/m^2 .

The visual effect due to the pupillary hippus is a sort of “pulsation” of the glare pattern. The effect is easily included in

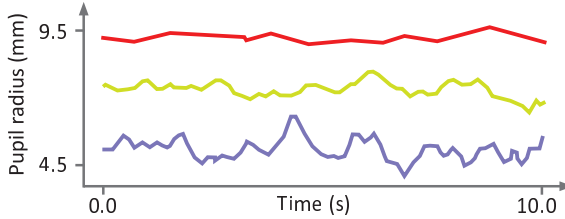


Figure 3: Change of pupil size over time for 3 different adaptation levels, which effectively depend on of the glare source strength. Bright conditions result in stronger oscillations.

our glare model by changing the size of the aperture according to Eqs. 1 and 2. In Eq. 1, value noise with three octaves [EMP*03] gave us plausible results. We use time-damped average screen intensity to approximate the field luminance [DD00].

3.3. The Lens

The lens is an important source of intraocular scattering as it accounts for about 40% of the forward scattering (cf. Table 1). Close investigation of the refractive index of lens fiber membranes [MvMVvdB02, MB06] has shown that they produce significant scattering, and that they are regularly spaced in the lens cortex. This high spatial order of the lens fiber lattice increases the transparency of the lens, but is also a diffraction grating which produces the lenticular halo. The refractive index of the fiber membranes decreases towards the center of the lens. This is why the grating is only significant in the lens cortex (as illustrated in the upper right corner of Figure 2). Our wave optics model easily accounts for the light diffraction on such a grating pattern.

Recently, the ciliary corona has been ascribed to randomly distributed particles in the lens [vdBHC05]. Van den Berg et al. explain the sharp needles to be the result of a seamless alignment of scaled copies of the same diffraction pattern originating from light of different wavelengths. However, Hemenger [Hem92] provides some theoretical evidence that the randomly distributed particles in the lens are too small to produce the ciliary corona on their own. Originally, Simpson [Sim53] suggested that the ciliary corona is due to particles situated in the vitreous, whose size is comparable to the larger particles in the lens nucleus [ASD*01]. This strongly suggests that the ciliary corona is produced by a combination of the few larger particles of the lens nucleus together with particles in the vitreous humor.

In this work we therefore consider both types of particles and simulate their motion, which is argued to be the main cause of temporal fluctuations observed in the ciliary corona. The motion of the particles in the lens is caused by lens deformations due to accommodative microfluctuations and is quantitatively different from the motion of the particles in

the vitreous humor which is mostly inertia-driven. At first we model the motion of lens particles and in the following section we describe the vitreous particles in more detail.

The human lens has been extensively investigated by physiologists and recently, elaborate numerical finite-element models for the lens' geometry were proposed [BJC02]. We use a simplified two-dimensional deformation model, assuming a radially symmetric lens with heuristic uniform deformation properties (spring stiffness) and a uniform discretization. We denote this deformation as $f(\mathbf{x})$, a mapping from two-dimensional coordinate \mathbf{x} to deformed two-dimensional coordinates. The deformation is first computed over a coarse discrete grid using a mass-spring system (cf. Fig. 4) yielding a discrete approximation \bar{f} to f . To apply f to a high number of lens particles in the continuous three-dimensional domain we use bi-linear interpolation from \bar{f} . To this end, every particle stores a random \mathbf{x} located inside the lens volume (using rejection sampling) and a random ϕ , which is an angle around the axis of symmetry. At runtime, we look up $f(\mathbf{x})$ for every particle at \mathbf{x} in \bar{f} and map it from cylindrical to Cartesian space.

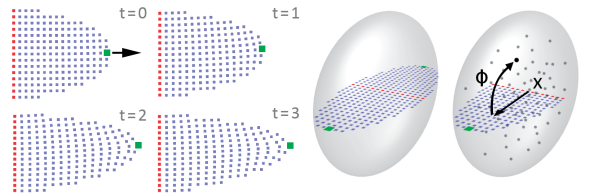


Figure 4: Left: The lens deformation model simulating ciliary muscle contraction (green element, arrow). Right: Mapping of the coarse 2D deformation to smooth 3D deformation.

The accommodation system is known to exhibit temporal variations even during fixation of a stationary stimulus which are due to adaptations of the ciliary muscle [GWG93]. We simulate these contractions of the ciliary muscle by moving a single element in \bar{f} . The oscillations caused by this reflex can be characterized by two principal components in their power-spectrum, one low-frequency (< 0.6 Hz) and one narrow high-frequency (between 1.3 and 2.1 Hz). Since the low-frequency component is known to vary with pupil size (more pronounced for larger size), we use the pupil size as determined in Eq. 2 to set the mean power of a low-frequency component generated with three-octave value noise according to experimentally acquired data [GWG93]. In practice, we use 17×17 elements for \bar{f} , 750 particles of varying size, and 200 gratings.

3.4. The Vitreous Humor

The vitreous humor contributes relatively little to the glare effect in terms of scattered light energy (cf. Table 1), and for this reason it is often ignored in glare research. However,

the contribution of scattering on particles in the vitreous to the ciliary corona is clearly visible in less central (less saturated) glare regions. This visibility is reinforced due to temporal effects which are extremely strong attractors of human attention especially in the visual periphery.

The vitreous humor is a slightly scattering viscoelastic body [Zim80]. This means that external forces (head movements, saccades) act on the vitreous humor such that it accelerates, rotates and comes to rest by strong damping. We model this behavior as a single rigid body with damped rotation dynamics, whose state is determined by angle and angular velocity. We set the damping to approximate the measurements by Zimmermann [Zim80]. We generate damped random forces to mimic saccades and integrate this system using forward Euler integration. The final particles are embedded at random but fixed locations inside this rigid body and do not move relatively to each other. Ansari et al. [ASD*01] have measured a three-dimensional map which describes the spatial distribution of particle sizes in the bovine vitreous which exhibits inhomogeneities similar to the human vitreous [Fan06]. The scatterers are thus modelled to have uniform random distribution throughout the vitreous.

3.5. The Retina

There are convincing arguments that the retina contributes to the intraocular scattering [VB64]. It is unfortunately difficult to model the retinal forward scattering directly using a particle distribution because the particles are intermingled with the receptor cells. To find out how the retinal scattering affects the glare pattern, [Nav85, vdBHC05] fitted a model to experimentally acquired glare functions [CIE99] which measure the combined effect of all the intraocular scattering. It turned out that fewer and larger particles (compared to measured particle sizes and frequencies) in the preretinal parts of the eye are an excellent way to approximate the measured glare functions. For this reason, we use fewer and larger particles in our model.

3.6. Eyelashes and Blinking

Eyelashes and blinking can result in long *streaks* in the glare pattern. We model blinking in the same way as Kakimoto et al. [KMN*04] by using bitmaps of eyelids and eyelashes. However, given our dynamic framework, we can produce animated blinking by moving the eyelashes against the pupil. In addition, we simulate squinting which is a normal reaction to a strong, discomforting glare source. It decreases the retinal illumination (and thus the discomfort) since the eyelids cut off the aperture and the eyelashes scatter the incident illumination [STH03]. Squinting is modeled by keeping the bitmaps closed by a constant amount.

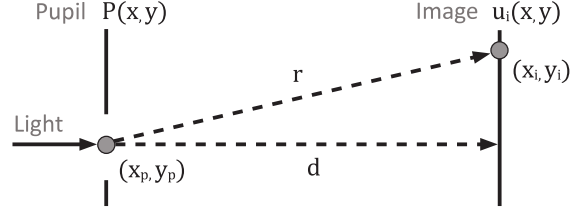


Figure 5: Schematic view of an optical system

4. Wave-Optics Simulation of Light-Scattering

To simulate the scattering at obstacles within the different anatomical structures of the eye, we use an approach based on wave-optics similar to [vdBHC05] and [KMN*04]. Even though the underlying theory is rather complicated, the implementation of scattering even on complex apertures is often simple and generally boils down to taking the Fourier transform (FT) of an aperture function. Considering the human eye as a simplified optical system (Fig. 5) with an aperture (pupil) and a image plane (retina), we obtain the diffraction pattern for particles and gratings within the lens and the cornea as well as for the eyelashes by computing the incident radiance following the Fresnel approximation to Huygen's principle [Goo05] given by

$$\begin{aligned} L_i(x_i, y_i) &= K \left| \mathcal{F} \{ P(x_p, y_p) E(x_p, y_p) \}_{p=\frac{x_i}{\lambda d}, q=\frac{y_i}{\lambda d}} \right|^2 \quad (3) \\ K &= 1/(\lambda d)^2 \\ E(x_p, y_p) &= e^{i \frac{\pi}{\lambda d} (x_p^2 + y_p^2)} \end{aligned}$$

for the coordinates (x_i, y_i) at the retina assuming unit-amplitude, homogeneous incident light. Here $P(x_p, y_p)$ is the aperture function for the pupil, giving the opacity of each point in the pupil (0 transparent, 1 opaque), λ is the wavelength of the light, d the distance between pupil and retina and \mathcal{F} denotes the Fourier transform that is evaluated at coordinates $(p, q) = (\frac{x_i}{\lambda d}, \frac{y_i}{\lambda d})$ (for a derivation, see Appendix A).

In contrast to [KMN*04] who use Fraunhofer diffraction, we use the more general Fresnel equation which contains Fraunhofer diffraction as a special case (we consider Fresnel diffraction as more appropriate, due to the relatively short distance between pupil and retina [Hec98]). In practice, the aperture function is modified before the FT by complex multiplication with the exponential given in Eq. 3 which produced more realistic results in our simulations (Fig. 6).

Simulating the scattering at particles in the vitreous is more complicated because their distance to the retina varies much more. A physically correct approach would be to compute separate Fresnel-diffraction patterns for each of these particles (because they differ in their distance to the retina) and add them up on an amplitude basis (J. Goodman, pers. comm.). However, this would involve costly operations that depend on the number of particles. Working towards a real-

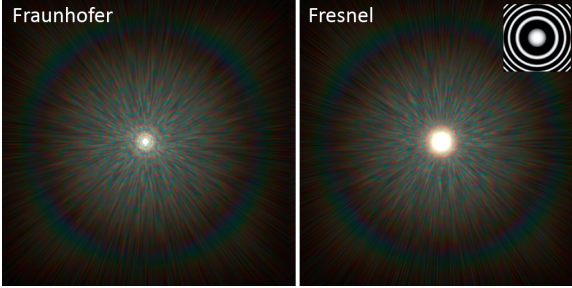


Figure 6: Comparison of Fraunhofer and Fresnel diffraction patterns. The Fresnel solution produces a more pronounced PSF. The term E from Eq. 3 is shown in the upper right corner.

time technique, we therefore compared a single-plane (where we project the particles in the vitreous directly into the pupil-plane) with a more correct multiple-plane approach (where we compute and add multiple diffraction patterns at different distances). Fig. 7 gives an impression of the difference of the two approaches. Judging the observable differences to be negligible, we chose to implement a single-plane approach to facilitate renderings that run in real-time even though this constitutes a physically incorrect simplification.

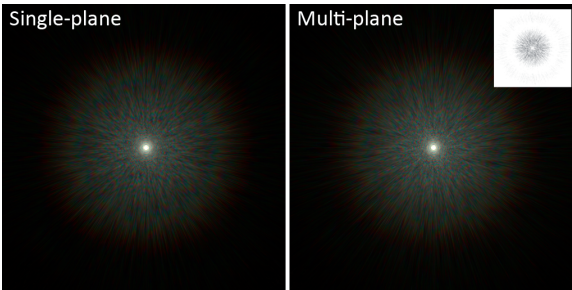


Figure 7: Single-plane (Left, 52.4 fps) and multiple-plane diffraction (Right, 32.1 fps) are perceptually equivalent (the difference is in the upper right corner). Using an individual plane for every particle would require 8 s/frame.

5. Implementation

We implemented our model to run in real-time entirely on recent graphics hardware (GPUs). Despite the involved theory, temporal glare is easily and efficiently implemented: Draw a few basic drawing primitives, apply an FFT, and do a special kind of blur. This already constitutes a temporal glare pipeline (cf. Fig. 8). The following paragraphs provide the details.

Human Aperture Model We simulate the aperture of the human pupil by drawing basic primitives into a texture. All primitives are rendered using 2×2 or more super-sampling.

This helps suppressing aliasing in time and space which would be exaggerated by the FFT. Fig. 9 shows partial PSFs that include only subsets of our aperture model in order to show how the individual parts contribute to the result.

Particles from the lens and the vitreous are projected orthogonally onto their aperture plane and drawn as 2D circles of equal size and color. Our implementation uses two sets of parameters. Static parameters encode subject-dependent variables: the number of particles, eye size and others. Dynamic parameters are updated for every frame: the blink state, the field luminance, the observer motion and others.

First, according to the blink state, we draw the eyelashes and eyelids as textured quads. Next, the pupil (cf. Sec. 3.2) is drawn as a 2D white circle on top of a black background. The radius of this circle is computed by our hippus model (cf. Eq. 1) using the field luminance. The next pass adds the lens (cf. Sec. 3.3) particles. Then gratings (Sec. 3.2) are drawn as lines of a few pixels thickness. Finally, the particles of the vitreous humor are simulated (cf. Sec. 3.4) and drawn.

Fresnel Diffraction The Fresnel diffraction of an aperture texture is computed in two steps. First, the aperture texture is multiplied by the complex exponential E (from Eq. 3) which we pre-compute and store in a static texture. Second, a recent GPU FFT [MA03] is applied to the aperture texture computing the \mathcal{F} -term from Eq. 3. After final normalization by K , the output is the monochromatic PSF F_λ .

Chromatic Blur The colorful appearance of glare can be modeled in a simple and efficient way [vdBHC05]. We exploit, the fact that a monochromatic PSF F_{λ_2} at wavelength λ_2 equals another monochromatic PSF F_{λ_1} for wavelength λ_1 whose argument is scaled by $\frac{\lambda_1}{\lambda_2}$ (cf. Eqn. 3):

$$F_{\lambda_2}(\mathbf{x}) = F_{\lambda_1}\left(\frac{\lambda_1}{\lambda_2}\mathbf{x}\right).$$

This equation is only strictly true in the Fraunhofer approximation. In the more exact Fresnel approximation, we would have to recompute the term E of Eq. 3, and thus also the FFT, for each wavelength. To avoid an FFT per wavelength and uphold real-time frame rates, we compute E for a single wavelength $\lambda_1 = 575\text{ nm}$ (in the middle of the visual spectrum since the error is smaller the closer λ_2 is to λ_1) and use this E for all wavelengths. The result is still a significant improvement over Fraunhofer diffraction (which assumes $E = 1$ for all λ).

We compute the spectral PSF F_s for a light with spectrum $s(\lambda)$ as a sum of n scaled copies of $F_{575\text{ nm}}$ as:

$$\begin{aligned} F_s(\mathbf{x}) &= \sum_{i=0}^{n-1} s(\lambda_i) F_{575\text{ nm}}(\mathbf{x}_i) \\ \lambda_i &= 380\text{ nm} + i \frac{770\text{ nm} - 380\text{ nm}}{n} \\ \mathbf{x}_i &= \mathbf{x} \frac{575\text{ nm}}{\lambda_i}. \end{aligned}$$

A fragment program computes F_s by summing n look-ups at

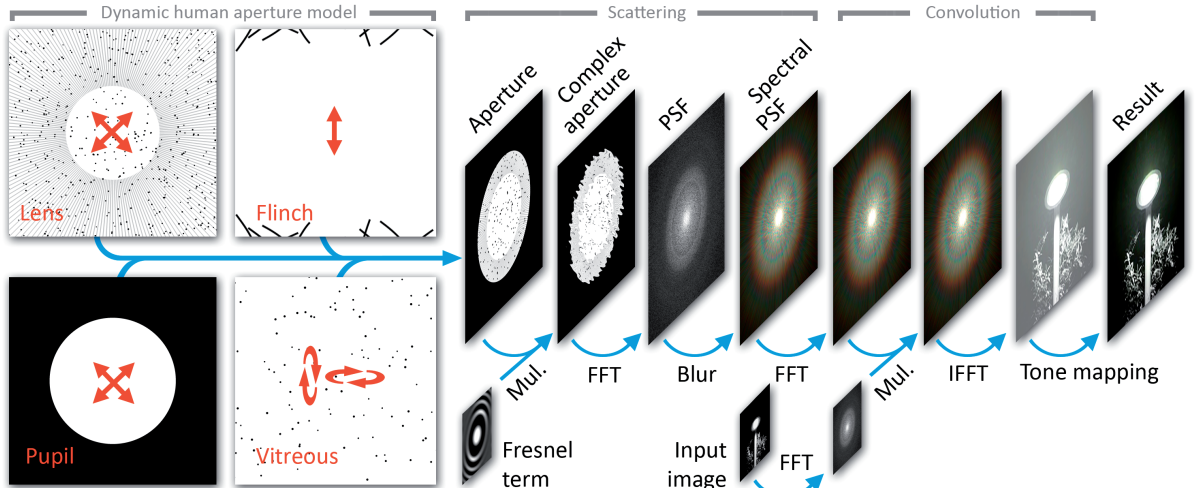


Figure 8: The temporal glare pipeline. The blue arrows are GPU shaders that transform one or multiple input textures (rectangles) into one or multiple output textures.

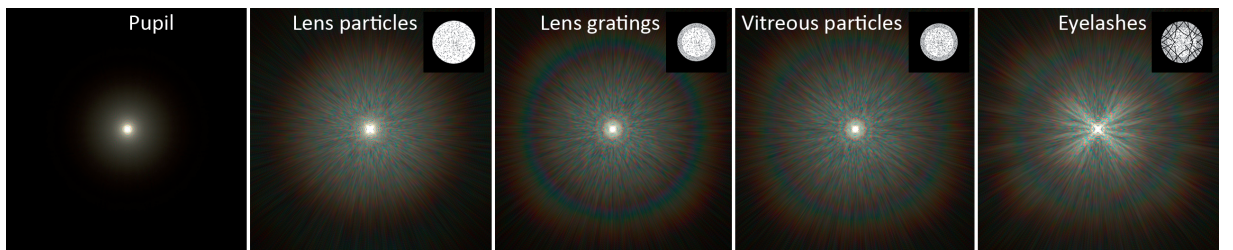


Figure 9: Adding scatterers from left to right. Vitreous and lens scattering looks similar, but have different dynamics.

different locations in the texture holding $F_{575\text{nm}}$. Each look-up is multiplied by the corresponding spectral value $s(\lambda_i)$. We use bi-linear interpolation to read the discrete $F_{575\text{nm}}$ at continuous sample locations \mathbf{x}_i . We use XYZ color space to represent s and F_s , and $n = 32$ resulted in the best tradeoff between quality and speed. Fig. 1 shows a RGB PSF.

Convolution We convolve the output image with this RGB PSF. This is different from previous methods, that only used billboards composed onto single bright pixels. Using the FT convolution theorem we compute the convolution as the multiplication of the FFT of the PSF and an FFT of the output image. The computation is done for all RGB channels in parallel using suitable internal texture formats. Applying a final inverse FFT to all channels yields the HDR input image “as seen” from our dynamic human eye model. Fig. 10 compares the convolution and billboard-based approaches. Note that such distinct appearance of the ciliary corona needles as shown in Figs. 1 and 10 (left) is typical for bright light sources with angular extent below 20 minutes of arc (the ray-formation angle [Sim53]). Larger light sources superimpose the fine diffraction patterns that constitute the needles

of the ciliary corona. This leads to a washing out of their structure as shown in Fig. 10 (right). However, the temporal glare effect is still visible because the superimposed needles fluctuate incoherently in time.

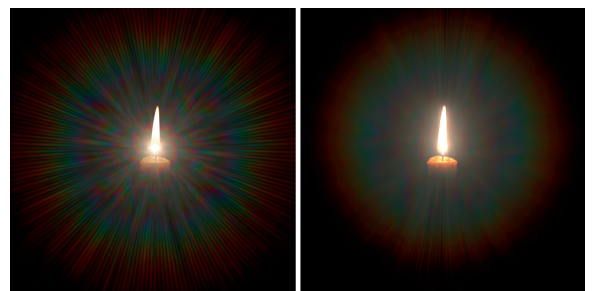


Figure 10: PSF applied using (left, 52.4fps) billboards and (right, 30.2fps) the convolution we propose. The results are substantially different for this candle. Using convolution, the horizontal needles of the ciliary corona blur out while the vertical needles remain unaffected.

One simple performance optimization is to pre-compute an animation cycle of RGB PSFs or to omit the convolution [KMN^{*}04]. Dynamic textures [SDW01] could be used to generate a faithful billboard approximation to dynamic glare with marginal overhead over static glare patterns e.g. for a game. Nevertheless, we use convolution in all our results.

Final Display For final display we apply a gamma mapping ($\gamma = 2.2$). While more advanced tone mapping operators could be used instead, we have chosen this simple approach because it gave us the most reliable and consistent results.

6. Results

Our method results in perceptual improvements as shown by a user study (cf. Sec. 6.1) with stimuli running at real-time frame rates (cf. Sec. 6.2).

6.1. Perceptual Study

To investigate the perceptual quality of our simulations, we conducted a psychological study comparing the effect of dynamic and static glare renderings in terms of realism, attractiveness and brightness. To provide a standardized setting for the preference study, subjects were simultaneously presented with two images of the same scene where each of the displays was either enhanced by application of dynamic or static glare or not. All possible combinations were presented for each scene. A range of different scenes representing divergent applications (natural images and computer-generated scenes) was chosen to ensure external validity (cf. Fig. 11). Subjects were asked to choose one of the two displays in a classical two-alternative-forced-choice (2-AFC) task according to one of three instructions: they had to judge which of the two images was brighter, more attractive or more realistic separately and in randomized order. The currently required task was indicated above the display in each trial. 10 naïve and paid subjects participated in the experiment and were seated at distance of 1m from the display. Each image occupied a visual angle of ≈ 10 vis. deg.

The study shows mixed results in terms of realism and attractiveness (see Fig. 12). The ratings within the individual observer were quite reliable (typically $r = .8$), but they show a large inter-individual variance. This is well explained by the fact that the glare phenomenon is a very personal experience that differs vastly between subjects (due to varying anatomy). This emphasizes, that a final glare rendering is never going to be completely realistic for the whole audience and that care should be taken to choose moderate parameter values for optimal effects. Another moderating factor was the scene to which the glare was applied. While the majority found dynamic glare most attractive for “Gem” and “Trees”, it was mostly disliked for “Park” and “Bridge” (see Fig. 11).

In the vast majority of trials, subjects reported to perceive dynamic glare as brighter than static ($\chi^2 = 72.2, p < .01$)

and control ($\chi^2 = 145.8, p < .01$) in all scenes. Because of the clear advantage of stronger perceived brightness for dynamic glare-rendering that was established in our study qualitatively, we additionally collected preliminary data from 4 subjects to quantify this effect. The psychophysical measurement of perceived glare brightness is methodologically difficult and results in a large intra- and inter-subject variance. We therefore applied an optimized double-adjustment method as previously proposed [YIMS08]. Subjects had to adjust the brightness of two spots simultaneously to match the perceived brightness of the centered target (which was either without, with static, or with dynamic glare). The mean value of both adjustments was used as the measured perceived luminance of the target. Subjects performed this task for the three different conditions (static, dynamic, control) and two different intensities of the target glare-rendering. The results are plotted in Fig. 12, and they show that both dynamic and static glare produced a boost in increased brightness relative to the control condition ($F(2, 4) = 8.22, p < .05$). The apparent advantage of the dynamical over the static glare rendering is not significant due to missing statistical power.

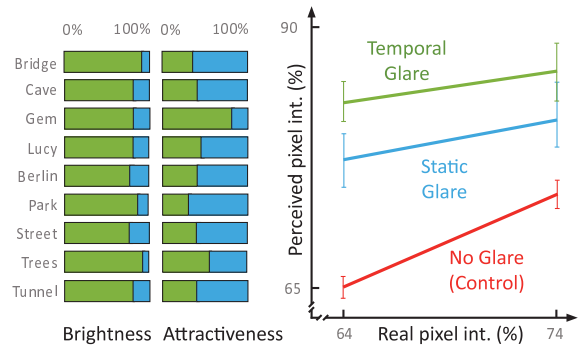


Figure 12: Left: Relative frequency of decisions for dynamic (green) and static (blue) glare. While dynamic glare is generally perceived as brighter, perceived attractiveness depends strongly on the individual scenes. Right: Subjects were well able to adjust the brightness to match control stimuli but perceived a boost in brightness for static and dynamic glare.

6.2. Performance

Table 2 presents performance numbers for our technique on an 2.4 GHz CPU with an NVIDIA GeForce 8800 GTX.

Size	Aperture	Diffraction	Display	Overall
256	5.2 ms	2.7 ms	1.1 ms	9.0 ms
512	11.8 ms	4.8 ms	1.8 ms	18.4 ms
1024	36.5 ms	13.8 ms	4.8 ms	55.1 ms

Table 2: Varying the PSF resolution and timing breakdown. For these timings, we used 2×2 super-sampling of the aperture, 32 samples for the RGB PSF, and no convolution.

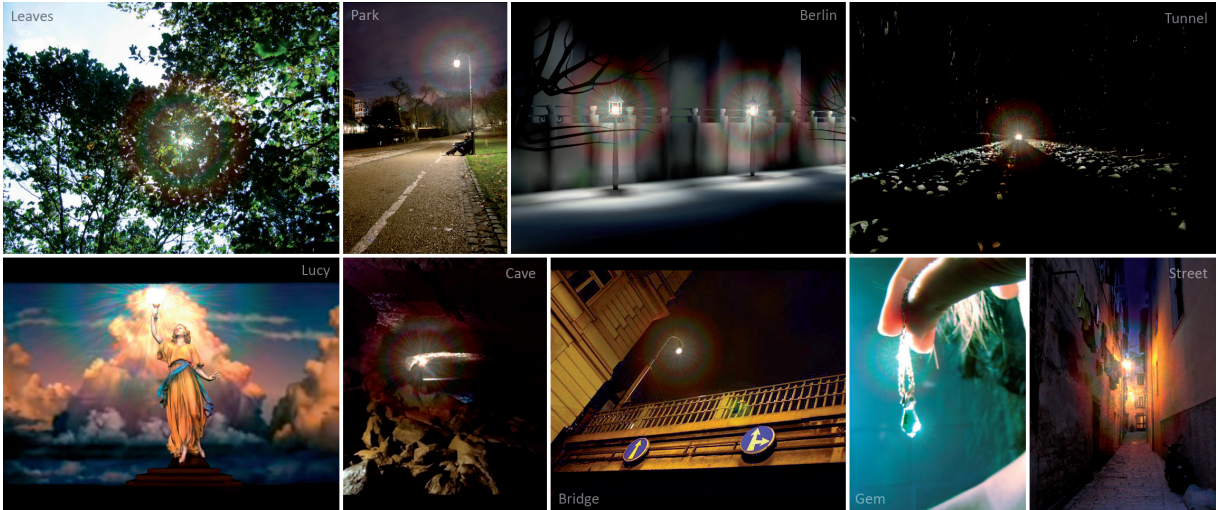


Figure 11: The nine stimuli used in the experiment. Please see the video for animated versions.

7. Conclusions

In this paper we proposed a model for the dynamics of the human eye and how they add temporal variation to the perceived glare-pattern. The method has a solid basis in eye anatomy and wave optics but remains practical as we demonstrate by implementing it in real-time on recent GPU hardware. A psychophysical study has shown that it improves perceived brightness, suggesting its applicability in a tone-mapping context. Since glare is a phenomenon intrinsic to the individual eye for which no ground truth can be obtained, its validation remains a challenging task. We plan to conduct a more detailed study, including more participants to better understand in which conditions temporal glare is important and where not and how individual components of our model contribute to the final result. Future work could elaborate the glare model, e.g. by including real-time subject information like gaze direction.

Acknowledgements

We acknowledge the support of Thomas Van den Berg, Joseph W. Goodman (communications), Matthias Hullin (proof reading), Rafal Mantiuk (proof reading), Mateusz Malinowski (video textures), Tobias Penzkofer (literature), Ramesh Raskar (discussions), Thomas Schultz (proof reading), Kaleigh Smith (proof reading) and flickr users „kuyman” and „Face it” (images).

References

- [ASD*01] ANSARI R. R., SUH K. I., DUNKER S., KITAYA N., SEBAG J.: Quantitative Molecular Characterization of Bovine Vitreous and Lens with Non-invasive Dynamic Light Scattering. *Experimental Eye Research* 73, 6 (2001), 859–866.
- [BC64] BOYNTON R. M., CLARKE F. J. J.: Sources of Entoptic Scatter in the Human Eye. *Journal of the Optical Society of America* 54, 1 (January 1964), 110–119.
- [Ben71] BENEDEK G. B.: Theory of Transparency of the Eye. *Applied Optics* 10, 3 (March 1971), 459–473.
- [BJC02] BURD H., JUDGE S., CROSS J.: Numerical modelling of the accommodating lens. *Vision Research* 42, 18 (2002), 2235–2251.
- [CIE99] CIE: *Collection 1999: Vision and Colour, Physical Measurement of Light and Radiation*. Tech. Rep. 135–1999, Commission Internationale de l’Eclairage, 1999.
- [DD00] DURAND F., DORSEY J.: Interactive Tone Mapping. In *Proceedings of the Eurographics Workshop on Rendering Techniques 2000* (London, UK, 2000), Springer-Verlag, pp. 219–230.
- [EMP*03] EBERT D. S., MUSGRAVE F. K., PEACHEY D., PERLIN K., WORLEY S.: *Texturing & Modeling: A Procedural Approach*, third ed. Morgan Kaufmann Publishers, 2003.
- [Fan06] FANKHAUSER II F.: Dynamic Light Scattering in Ophthalmology: Results of In Vitro and In Vivo experiments. *Technology & Health Care* 14, 6 (2006), 521–535.
- [FMF86] FREUND D. E., MCCALLY R. L., FARRELL R. A.: Effects of Fibril Orientations on Light Scattering in the Cornea. *Journal of the Optical Society of America A* 3, 11 (November 1986), 1970–1982.
- [Fry91] FRY G. A.: The Relation of Pupil Constriction Experienced Under Discomfort Glare. In *Proceedings of the First International Symposium on Glare* (1991), Adrian W., (Ed.), Lighting Research Institute, pp. 173–181.
- [Goo05] GOODMAN J.: *Introduction To Fourier Optics*. Roberts & Co, 2005.
- [GWG93] GRAY L. S., WINN B., GILMARTIN B.: Accommodative microfluctuations and pupil diameter. *Vision Research* 33, 15 (1993), 2083–2090.
- [Hec98] HECHT E.: *Optics*, 3rd edition ed. MA: Addison-Wesley Publishing Company, 1998.
- [Hem92] HEMENGER R.: Sources of Intraocular Light Scatter from Inversion of an Empirical Glare Function. *Applied Optics* 31, 19 (July 1992), 3687–3693.

- [Kaw05] KAWASE M.: Practical Implementation of High Dynamic Range Rendering. In *Game Developers Conference* (2005).
- [KMN*04] KAKIMOTO M., MATSUOKA K., NISHITA T., NAE-MURA T., HARASHIMA H.: Glare Generation Based on Wave Optics. In *PG '04: Proceedings of the 12th Pacific Conference on Computer Graphics and Applications (PG'04)* (Washington, DC, USA, 2004), IEEE Computer Society, pp. 133–142.
- [KRFF95] KÖNZ F., RICKA J., FRENZ M., FANKHAUSER F.: Dynamic Light Scattering in the Vitreous: Performance of the Single-Mode Fiber Technique. *Optical Engineering* 34, 8 (August 1995), 2390–2395.
- [LRP97] LARSON G. W., RUSHMEIER H., PIATKO C.: A Visibility Matching Tone Reproduction Operator for High Dynamic Range Scenes. *IEEE Transactions on Visualization and Computer Graphics* 3 (1997), 291–306.
- [MA03] MORELAND K., ANGEL E.: The FFT on a GPU. In *HWWS '03: Proceedings of the ACM SIGGRAPH/EUROGRAPHICS conference on Graphics hardware* (Aire-la-Ville, Switzerland, Switzerland, 2003), Eurographics Association, pp. 112–119.
- [MB06] MICHAEL R., BARRAQUER R. I.: *Refractive Index of Lens Fiber Membranes in Different Parts of the Crystalline Lens: Impact on Lens Transparency*. Nova Science Publishers, Inc., 2006, ch. 7, pp. 167–181.
- [MPC02] MURRAY I. J., PLAINIS S., CARDEN D.: The Ocular Stress Monitor: A New Device for Measuring Discomfort Glare. *Lighting Research & Technology* 34, 3 (2002), 231–242.
- [MS44] MOON P., SPENCER D. E.: On the Stiles-Crawford Effect. *Journal of the Optical Society of America* 34, 6 (June 1944), 319–329.
- [MvMVvdB02] MICHAEL R., VAN MARLE J., VRENSEN G. F., VAN DEN BERG T. J.: Refractive Index of Lens Fiber Membranes in Different Parts of the Crystalline Lens. In *Proceedings of SPIE* (June 2002), vol. 4611, pp. 159–164.
- [Nav85] NAVARRO R.: Incorporation of Intraocular Scattering in Schematic Eye Models. *Journal of the Optical Society of America A* 2, 11 (1985), 1891–1894.
- [NKN90] NAKAMAE E., KANEDA K., OKAMOTO T., NISHITA T.: A Lighting Model Aiming at Drive Simulators. In *SIGGRAPH '90: Proceedings of the 17th annual conference on Computer graphics and interactive techniques* (New York, NY, USA, 1990), ACM, pp. 395–404.
- [RAWV08] RASKAR R., AGRAWAL A., WILSON C. A., VEER-ARAGHAVAN A.: Glare Aware Photography: 4D Ray Sampling for Reducing Glare Effects of Camera Lenses. *ACM Trans. Graph.* 27, 3 (2008), 1–10.
- [Rok93] ROKITA P.: A Model for Rendering High Intensity Lights. *Computers & Graphics* 17, 4 (1993), 431–437.
- [RPWD05] REINHARD E., WARD G., PATTANAIK S., DEBEVEC P.: *High Dynamic Range Imaging: Acquisition, Display, and Image-Based Lighting*. Morgan Kaufmann Publishers Inc., San Francisco, CA, USA, 2005.
- [SDW01] SOATTO S., DORETTO G., WU Y. N.: Dynamic textures. In *International Journal of Computer Vision* (2001), pp. 439–446.
- [Sim53] SIMPSON G.: Ocular Haloes and Coronas. *Br. J. Ophthalmol.* 37, 8 (1953), 450–486.
- [SSZG95] SPENCER G., SHIRLEY P., ZIMMERMAN K., GREENBERG D. P.: Physically-Based Glare Effects for Digital Images. *Computer Graphics* 29, Annual Conference Series (1995), 325–334.
- [STH03] SHEEDY J. E., TRUONG S. D., HAYES J. R.: What are the visual benefits of eyelid squinting? *Optometry and Vision Science* 80, 11 (2003), 740–744.
- [VB63] VOS J. J., BOOGAARD J.: Contribution of the Cornea to Entoptic Scatter. *Journal of the Optical Society of America* 53, 7 (July 1963), 869–873.
- [VB64] VOS J. J., BOUMAN M. A.: Contribution of the Retina to Entoptic Scatter. *Journal of the Optical Society of America* 54, 1 (1964), 95–100.
- [vdB95] VAN DEN BERG T. J. T. P.: Analysis of intraocular straylight, especially in relation to age. *Optometry and Vision Science* 72, 2 (1995), 52–59.
- [vdBHC05] VAN DEN BERG T. J. T. P., HAGENOW M. P. J., COPPENS J. E.: The Ciliary Corona: Physical Model and Simulation of the Fine Needles Radiating from Point Light Sources. *Investigative Ophthalmology and Visual Science* 46 (2005), 2627–2632.
- [vdBIdW91] VAN DEN BERG T. J. T. P., IJSPEERT J. K., DE WAARD P. W. T.: Dependence of Intraocular Straylight on Pigmentation and Light Transmission Through the Ocular Wall. *Vision Research* 31, 7–8 (1991), 1361–1367.
- [WS82] WYSZECKI G., STILES W. S.: *Color Science: Concepts and Methods, Quantitative Data and Formulae*, second ed. John Wiley & Sons, Inc., 1982.
- [YIM08] YOSHIDA A., IHRKE M., MANTIUK R., SEIDEL H.-P.: Brightness of Glare Illusion. In *Proceedings of ACM Symposium on Applied Perception in Graphics and Visualization* (Los Angeles, CA, USA, 2008), ACM, pp. 83–90.
- [YYG*93] YUAN R., YAGER D., GUETHLEIN M., OLIVER G., KAPOOR N., ZHONG R.: Controlling Unwanted Sources of Threshold Change in Disability Glare Studies: A Prototype Apparatus and Procedure. *Optometry & Vision Science* 70, 11 (1993), 976–981.
- [Zim80] ZIMMERMAN R. L.: In Vivo Measurements of the Viscoelasticity of the Human Vitreous Humor. *Biophysical Journal* 29, 3 (March 1980), 539–544.

Appendix A: Derivation of the Fresnel Approximation

One way to derive the Fresnel approximation is using Huygen's principle, which states that a wavefront can be extended by assuming an infinite number of wave-emitters along the wavefront. Assuming the setup in Fig. 5, the intensity of the light in the image plane $u_i(x_i, y_i)$ is expressed as a double integral over the light incident on the pupil $u_p(x_p, y_p)$ where a new harmonic, spherical wave is emitted at each point

$$u_i(x_i, y_i) = \frac{d}{i\lambda} \iint_P u_p(x_p, y_p) \frac{\exp(ikr)}{r^2} dx_p dy_p ,$$

where d is the distance between the pupil and image planes, r is the distance to the source, P the pupil-area over which is integrated, and $k = 2\pi/\lambda$ is the wave number. The Fresnel approximation follows if r is substituted by the first terms of its binomial expansion such that the terms under the integral can be rearranged and expressed as the Fourier transform (FT) of the product of the pupil function and the complex exponential. Assuming unit-amplitude, homogeneous light, we have:

$$u_i(x_i, y_i) = -\frac{i \exp(ikd) \exp(\frac{ik}{2d}(x_i^2 + y_i^2))}{\lambda d} \mathcal{F}\{P(x_p, y_p)E(x_p, y_p)\}$$

Because we are interested in radiance $L_i(x_i, y_i) = |u_i(x_i, y_i)|^2$, the term in front of the FT becomes a constant, yielding Eq. 3.